Chapter 3

Mathematical interpretation of wave propagation, standing wave resonance and absorption in a metasurface absorber

3.1. Introduction

The theory of absorption based on Fabry-Perot resonance provides a better mathematical insight of wave propagation in terms of multiple reflections of waves between the top and metallic bottom plates by deriving the expressions of amplitude and phase conditions. The absorption in the structure has been explained in the light of interference of the multiple reflected waves, providing a standing wave between the top and bottom metallic plates [65-68]. One of the initial works in this direction have been carried out in [69-70], where the total electric field inside the dielectric cavity has been derived to explain the multiband absorption in the metasurface absorber. However, in this paper, the authors did not discuss the formation of the magnetic field, and therefore, the power dissipation within the cavity could not be explained numerically. Further, analysis of absorption has been found to be applicable only for transverse magnetic (TM) polarized incident electromagnetic waves. Nevertheless, for a perfect absorber, the absorptivity should be almost identical under transverse electric (TE) and TM polarized incident waves. Hence, the theory applicable for a TM polarized incidence should also be applicable for a TE polarized incidence.

In this chapter, a complete mathematical model of absorption via multiple reflection of waves between the top and metallic bottom plates of the metasurface absorber has been carried out. The electromagnetic field component of the incident and reflected waves had been used to

derive the expression for the total electric and magnetic fields existing inside the dielectric cavity of the metasurface absorber. As a result, it is possible mathematically to explain the formation of standing wave resonance, surface current orientation, and absorption from the expression of the electric and magnetic fields. The effect of change in the polarization angle of the incident electromagnetic wave on the standing wave pattern and surface current orientation has also been done. The study suggests that the theory is equally applicable for TE as well as TM polarized incidence. All the mathematical aspects have been established through the validation of simulation data by analytical results, and it has been found subsequently that the theory is in good agreement with the analytical results.

3.2. Mathematical model of multiple reflections phenomenon

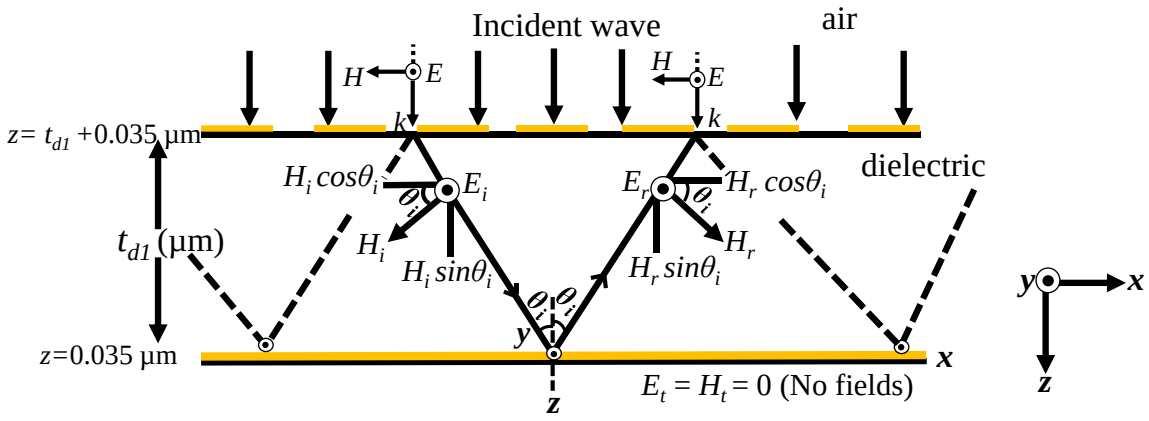

Fig. 3.1 Multiple interference inside the dielectric cavity of the metasurface absorber along with incident and reflected electric and magnetic field components.

To describe the theory, a schematic showing multiple reflections inside the dielectric cavity of the metasurface absorber is shown in Fig. 3.1. Initially, a transverse electric (TE) -polarized plane wave is considered, which is incident normally on the top layer of the metasurface. Due to the presence of gaps in the metallic structure, the wave diffracts obliquely inside the dielectric cavity and propagates while undergoing multiple reflections between the top and bottom metallic layers. Let the wave propagating along $+z$ -direction is incident obliquely inside the dielectric cavity at an angle θ_i. Considering the TE polarized wave, let the

polarization of the incident and reflected electric fields be perpendicular to the interface i.e., along $+y$-direction. From the directions of the electric field and wave vector, the orientation of the incident and reflected magnetic fields can be resolved, as shown in Fig. 3.1. The electric and magnetic fields for the incident electromagnetic wave can be written as equations 3.1-3.2, respectively.

$$\bar{E}_i = E_{io} e^{-j(\beta z \cos\theta_i + \beta x \sin\theta_i + \pi)} \hat{y} \tag{3.1}$$

$$\bar{H}_i = \frac{E_{io}}{\eta}(\sin\theta_i \hat{z} - \cos\theta_i \hat{x}) e^{-j(\beta z \cos\theta_i + \beta x \sin\theta_i + \pi)} \tag{3.2}$$

Here, β and η are respectively the propagation constant and intrinsic impedance of the dielectric. The phase reversal of the incident wave due to the reflection from the bottom metallic reflector is compensated with an additional phase of π in the incident wave equations. Accommodating proper sign changes, the electric and magnetic fields for the reflected wave can be written as provided in equations (3.3) and (3.4), respectively.

$$\bar{E}_r = E_{ro} e^{-j(-\beta z \cos\theta_i + \beta x \sin\theta_i)} \hat{y} \tag{3.3}$$

$$\bar{H}_r = \frac{E_{ro}}{\eta}(\sin\theta_i \hat{z} + \cos\theta_i \hat{x}) e^{-j(-\beta z \cos\theta_i + \beta x \sin\theta_i)} \tag{3.4}$$

Since the tangential components of the electric field oriented along $+y$-direction vanishes at the media interface due to the presence of the continuous metallic reflector at the bottom, by applying suitable boundary conditions, it can be found that $E_i = E_r$. Accordingly, the net electric field at any point within the dielectric cavity can be computed, as provided in equation 3.5.

$$E_y = -2jE_{io} e^{-j\beta x \sin\theta_i} \sin(\beta z \cos\theta_i) \tag{3.5}$$

Similarly, the net magnetic field within the dielectric cavity can be obtained by adding the incident and reflected magnetic fields. Both the components of magnetic fields have been evaluated and provided in equations 3.6-3.7.

$$H_x = -2\frac{E_{io}}{\eta}e^{-j\beta x\sin\theta_i}\cos\theta_i\cos(\beta z\cos\theta_i) \tag{3.6}$$

$$H_z = -2j\frac{E_{io}}{\eta}e^{-j\beta x\sin\theta_i}\sin\theta_i\sin(\beta z\cos\theta_i) \tag{3.7}$$

From the expression of the electric field, derived in equation 3.5, it can be observed that the electric field represents a travelling wave in $+x$-direction and a standing wave in z-direction. Similarly, from the expressions of the magnetic field components, derived in equations 3.6-3.7, it can be observed that the magnetic fields possess a propagating nature in $+x$-direction and a standing wave nature in z-direction. The derived electric and magnetic fields can be used to understand the power dissipation inside the cavity by determining the average Poynting vector. It is evident from the expressions of E_y and H_x that they are out of phase by 90^0; thus resulting in an average power of zero along z-direction [71]. On the contrary, the fields E_y and H_z are in phase and thus contribute an average power flow along $+x$-direction. In other words, it can be said that the wave which has diffracted inside the dielectric cavity propagates along $+x$-direction while undergoing multiple reflections between the top and bottom metallic plates, but with each set of incidence and reflection they dissipate all its power, while forming standing wave along z-direction.

To validate the theory, a metasurface absorber operating at 10 μm wavelength has been simulated in CST microwave studio. All the results have been evaluated at the absorbing wavelength viz., 10 μm. The top and side views of the unit cell of the metasurface absorber structure have been shown in Figs. 3.2(a) and 3.2(b), respectively. The side view of the unit cell of the metasurface absorber structure as shown in Fig. 3.2(b) comprises metallic reflector as bottom layer, dielectric as middle layer and metallic pattern as the top layer. The top metallic pattern does not have multiple layers, rather, it is one of the layers of the three-layered unit cell.

For the metallic structures gold has been chosen due to low ohmic loss, better chemical stability and ease of fabrication at smaller dimensions.

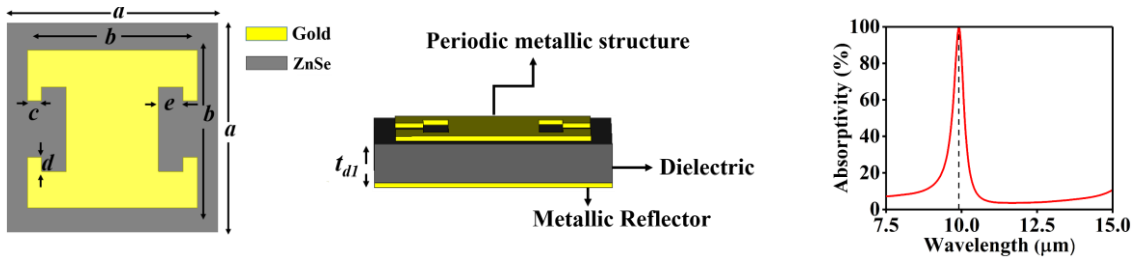

(a) (b) (c)

Fig. 3.2 Schematic of the (a) top and (b) side views of the unit cell of a metasurface absorber operating at 10 μm along with (c) the absorptivity response (a = 1.5 μm, b = 1.2 μm, c = 0.1 μm, d = 0.1 μm, e = 0.2 μm).

For a realistic model of metal characteristics at higher frequencies, the dielectric permittivity of gold has been modelled using the Drude expression model. For the dielectric, ZnSe has been selected due to its good thermal and mechanical property at the infrared frequencies. The dielectric constant of ZnSe at the frequency of operation has been taken from the experimental data given in. The geometrical dimensions of the unit cell have been optimized for maximum absorptivity at 10 μm, as mentioned in Fig. 3.2. The thickness of the dielectric cavity is, t_{d1} = 4.48 μm, whereas the thickness of metal plates at the top and bottom layers are 0.035 μm each, which is slightly greater than the skin depth of gold at the wavelength of absorption. The absorptivity response in Fig. 3.2(c) depicts that the structure offers near unity absorption at 10 μm when simulated employing periodic boundary conditions.

3.2.1. Standing wave resonance inside the dielectric

Initially, the variations of the real part of E_y and H_x components of the electromagnetic wave have been evaluated analytically along z-direction, encompassing the region between

$z = 0.035\mu m$ (bottom metallic reflector) to $z = (t_{d1} + 0.035)\mu m = 4.515\mu m$ (top metallic layer), as shown in Figs. 3.3(a) and 3.3(b), respectively.

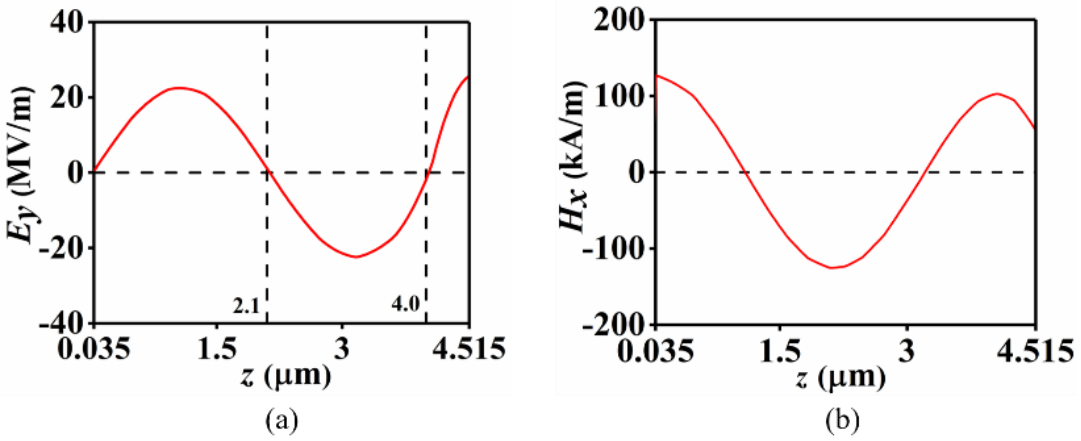

Fig. 3.3. Variations of real part of (a) E_y and (b) H_x field components (at the operating wavelength i.e., 10 μm*)* along z direction for the metasurface absorber whose unit cell is shown in Fig. 3.2.

It can be observed from Fig. 3.3 that the electric field (E_y) in z -direction represents a standing wave, as it varies according to the term $\sin(\beta z)$, derived in equation (3.5) whereas the magnetic field (H_x) in z -direction represents a standing wave, and varies according to the term $\cos(\beta z)$, as derived in equation (3.6). While evaluating the standing wave curve, we have ignored the term $\cos\theta_i$, considering the fact that the refractive index of ZnSe is more than twice compared to the refractive index of air, therefore the term $\cos\theta_i \approx 1$ (when angle θ_i is very small). The curve shown in Fig. 3.3 is for the case when the phase ϕ (polarization angle) of the incident electromagnetic wave is 0^0. However, it is possible that the wave which is incident normally on the top layer of the metasurface layer might have a change in its angle of polarization (ϕ). Hence, a subsequent study of the variation in the polarization angle of the incident electromagnetic wave on the standing wave patterns have been carried out and illustrated in Figs. 3.4(a) and 3.4(b), respectively. It can be observed from Fig. 3.4(a), that when

the value of ϕ changes from 0^0 to 90^0, the magnitude of the standing wave subsequently decreases. At $\phi = 90^0$, there is no standing wave formation, as can be seen from a zero magnitude curve of the electric field (E_y). Further increase in the value of ϕ leads to a subsequent rise in the magnitude curve, which reaches, to a maximum at $\phi = 180^0$.

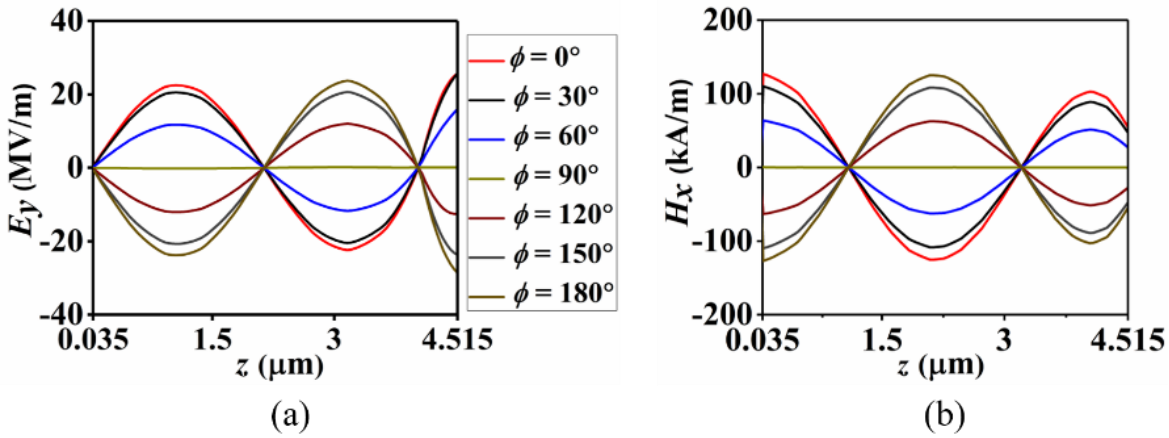

Fig. 3.4. Effect of change in the polarization angle of the incident electromagnetic wave on the standing wave pattern of (a) E_y and (b) H_x components.

3.2.2. Variation in the standing wave pattern for change in the polarization angle

The above phenomenon can be understood in the light of polarization angle variation. Initially, when the phase was 0^0, the orientation of the electric field was in y direction. Therefore, the magnitude of the electric field (E_y) was maximum. As the value of ϕ increases, the electric field start shifting towards x-direction, as can be seen from a decrease in the magnitude curve of the electric field. When the value of ϕ reaches 90^0, the electric field completely shifts its orientation from y to x, as evident from a zero magnitude curve of E_y component. Further increase in the value of ϕ to 180^0, results another rotation of electric field by a quadrature phase, i.e., from x to $-y$, as evident from a maximum magnitude curve (in negative phase).

The explanation presented above is for the case when the incident electromagnetic wave is TE-polarized. However, a perfect metasurface absorber should exhibits identical response for the TM-polarized incident waves too. Hence the theory of standing wave resonance which is applicable for a TE polarized incidence, should also be applicable for a TM polarized incidence. In order to verify this point, the effect of phase ϕ on the standing wave pattern for both TE and TM polarized incident waves have been evaluated, as shown in Figs. 3.5(a) and 3.5(b) respectively. It can be seen from Fig. 3.5(a) that when the incident electric field is TE polarized (i.e., in y direction), the E_y component of electric field has maximum magnitude for $\phi = 0^0$ and minimum (zero) magnitude for $\phi = 90^0$. In contrast, for a TM polarized incident wave (i.e., in x direction), the E_y component of electric field possesses minimum magnitude for $\phi = 0^0$ and maximum (zero) magnitude for $\phi = 90^0$, as shown in Fig. 3.5(b). Hence, the theory is equally applicable for a TM polarized incident wave too; nevertheless, the only change required is in the direction of the vectors of electric and magnetic fields.

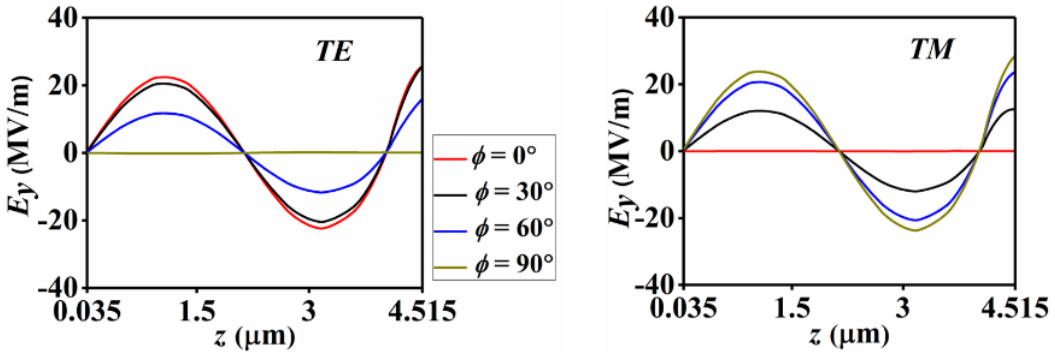

Fig. 3.5. Variation in the standing wave pattern for change in the polarization angle when the incident electromagnetic wave is (a) TE polarized and (b) TM polarized.

3.3. Study of Electric Field and Polarization Angle on the Orientation of Surface Currents

The tangential electric field at the top and bottom metallic plates induce electric currents, according to equation (3.8) and (3.9), respectively.

$$J_{top} = j\omega\varepsilon_{top}E_{y-top} \tag{3.8}$$

$$J_{bottom} = j\omega\varepsilon_{bottom}E_{y-bottom} \tag{3.9}$$

The directions of the surface current can be decided by the phase of the electric field (E_y) at the top and bottom metal plates together with the signs of the effective permittivity of the two plates, depicted from above equations. The dielectric permittivity of the top metasurface layer (ε_{top}) can be obtained by simulating the air-metal pattern-dielectric configuration. The simulated reflection and transmission coefficients data are then used to retrieve the dielectric permittivity of the top metasurface layer. It has been found that the dielectric permittivity of the top layer of the metasurface (ε_{top}) is always positive at the frequency of operation, as shown previously in chapter 2, [72] whereas the dielectric permittivity of bottom metallic layer (ε_{bottom}) is always negative, according to the Drude model. Hence, the sign of the effective permittivity of the top and bottom metallic plates is always opposite to one another. Considering the opposite signs of the dielectric permittivity, the direction of surface currents is then decided by the phase of the electric field (E_y) at the top and bottom metallic layers. For anti-parallel surface currents, the signs of J_{x-top} and $J_{x-bottom}$ should be opposite to each other, which is possible only when the phases of E_y at the top and bottom metallic plates are identical in nature. On the other hand, for parallel surface current, the signs of J_{x-top} and $J_{x-bottom}$ should be same, which is possible when the phase of E_y at the top and bottom metallic plates will be different. To validate this point, we have considered the curve of E_y , as shown in Fig. 3.3(a) (also displayed in the inset of Fig. 3.6) and analytically evaluated the surface currents for the

metasurface structure having various dielectric thickness; $t_{d1}=1.2\mu m$, $t_{d1}=1.8\mu m$, $t_{d1}=2.2\mu m$, $t_{d1}=2.8\mu m$, as illustrated in Figs. 3.6(a)-(d), respectively.

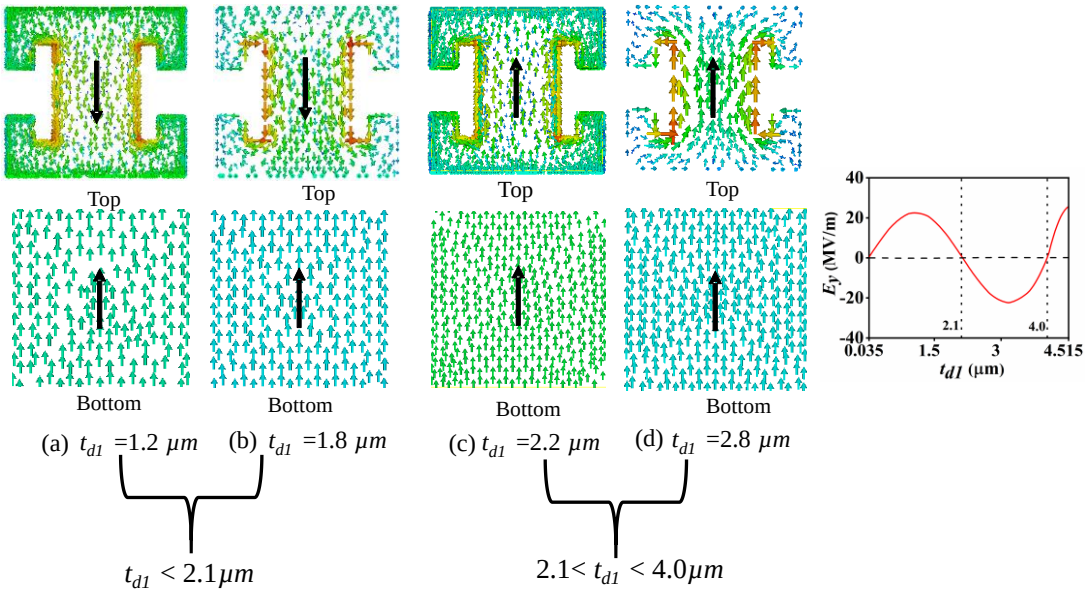

Fig. 3.6. Orientation of surface currents at the top and bottom metallic plates for dielectric thickness (a) 1.2 μm (b) 1.8 μm (c) 2.2 μm and (d) 2.8 μm (Inset depicts the curve of Fig. 3.3(a)).

It can be seen from the figure shown in the inset of Fig. 3.6, that for the metasurface structure having dielectric thickness $t_{d1}<2.1\mu m$, the electric field E_y has identical phase at the bottom metallic plate ($z=0.035\mu m$) as well as top metallic plate ($z=t_{d1}<2.1\mu m$). Thus, for any metasurface absorber structure having dielectric thickness $t_{d1}<2.1\mu m$, the surface currents at the top and bottom metallic plates will be anti-parallel to each other. In order to justify this point, we have studied the surface currents for dielectric thickness $t_{d1}=1.2\mu m$ and $t_{d1}=1.8\mu m$, as shown in Figs. 3.6(a) and 3.6(b), respectively and found that they are antiparallel to each other. Moreover, it can be seen from Fig. 3.3(a), that for metasurface structure having dielectric thickness in the range $2.1\mu m<t_{d1}<4.0\mu m$, the electric field at the top and bottom metallic

plates are out of phase with respect to each other, thereby providing parallel surface currents, as evident from Figs. 3.6(c) and 3.6(d), respectively.

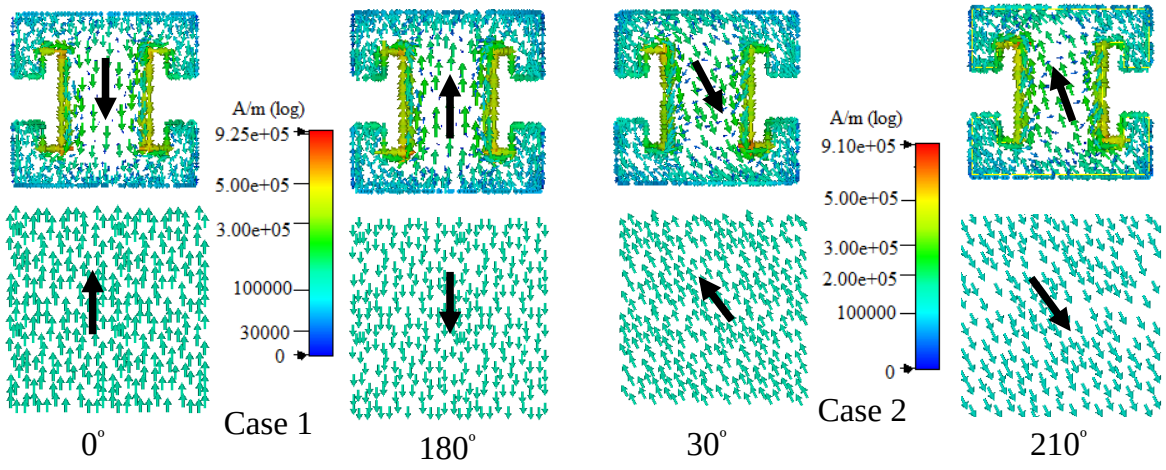

Fig. 3.7. Orientation of surface currents at the top and bottom metal plates for (a) case 1:- (0^0 and 180^0) (b) case 2:- (30^0 and 210^0).

The effect of change in the polarization angle on the orientation of surface currents have been evaluated in Fig. 3.7. From Fig. 3.4(a), it can be seen that the curve of the electric field (E_y) at the bottom ($z = 0.035\mu m$) and top ($z = 4.515\mu m$) metallic plates for $\phi = 0^0$ and $\phi = 180^0$ are exactly equal in magnitude, but opposite in phase. Henceforth, the surface current for $\phi = 0^0$ and $\phi = 180^0$ at the top and bottom metallic plate is exactly equal in magnitude but opposite in orientation, shown as case 1 of Fig. 3.7. Similarly, the orientation of surface current for $\phi = 30^0$ and $\phi = 210^0$ is exactly equal in magnitude but opposite in orientation, illustrated as case 2 of Fig. 3.7.

3.4. Conclusions

This work presents a complete mathematical model of the metasurface absorber structure where the incident electromagnetic wave undergoes multiple interference inside the dielectric cavity of the metasurface structure. The phenomenon of wave propagation, standing wave formation, and

absorption has been mathematically explained with the help of electric and magnetic fields. The theory provides a better mathematical insight of absorber where the role of each layer can be well understood. Our study of standing wave resonance with change in the polarization angle reveals the reason for decrease in the absorptivity response of a metasurface absorber with increase in the polarization angle. The propagation of waves via multiple reflections between top and bottom metallic plates of the metasurface absorber can be studied and explored further in the light of waveguide model for TE and TM polarized electromagnetic incidence. Theoretically the model should be applicable up to the UV range [73]. Beyond this wavelength (extreme UV, X-ray and gamma radiation), the electromagnetic radiations become ionizing which may cause ionization of atoms in the dielectric and the model should accordingly consider the ionization effect too.

CONTENTS

Chapter 4: Structural and mathematical analyses of a dual-sided metasurface for the design of multifucntional and bidirectional optoelectronics devices

Chapter 4

Structural and mathematical analyses of a dual-sided metasurface structure for the design of multifunctional and bidirectional optoelectronics devices

4.1. Introduction

Multifunctionality of electronic devices has been a long-lasting pursuit for the electronic system, especially if the functions are mutually exclusive from one another. Most of the metasurface devices are based on single-sided metasurface structure employing a periodic metallic pattern-dielectric-metal configuration, where the dielectric layer is sandwiched between the top layer comprising metallic pattern and bottom metallic plate. Such single-sided metasurface structures are mostly used as an absorber in stealth technology for reducing the radar cross section area [74-75]. However, the presence of metallic plate at the bottom completely blocks the entire frequency band. This causes a fatal problem in the wireless communication system, where apart from absorbing a certain band of frequency, another band of frequency needs to be transmitted to communicate with other remote devices. A multifunctional device that offers absorption and transmission in two separate bands of frequencies is referred as “rasorber” [76-77]. Most of them have used passive circuit elements such as resistance, inductance, capacitance for their realization [78-79]. Due to the presence of vias for the realization of inductance, such devices are difficult to realize in practice. Later, re-configurable rasorber based on PIN diode has been reported in [80], which switches the mode of operation from absorption to transmission by applying suitable bias voltage across the diode. However, the presence of PIN diode in the bottom makes only one layer re-configurable. In